References

[1] Nagano, M. and Watson, A. 'Ultra High Energy Cosmic Rays'. *Review of Modern Physics* **72**, 689 (2000).

[2] Kampert, K. 'Methods of Determination of the Energy and Mass of Primary Cosmic Ray Particles at Extensive Air Shower Energies'. *Journal of Physics G: Nuclear Physics* **27**(7), 1663 (2001).

[3] Kulikov, G. V. and Khristiansen, G. B. 'On the Size Spectrum of Extensive Atmosphere Showers'. *Journal of Experimental and Theoretical Physics* **35**, 635 (1958).

[4] Aglietta, M., Alessandro, B., Antonioli, P., et al. 'Study of the Cosmic Ray Primary Spectrum at $10^{15} < E_0 < 10^{16}$ eV with the EAS-TOP Array'. *Nuclear Physics B (Proceedings Supplemental)* **85**, 318 (2000).

[5] Longair, M. *High Energy Astrophysics*. Cambridge University Press, (1981).

[6] Auger, P. 'Extensive Cosmic Ray Showers'. *Review of Modern Physics* **11**, 288 (1939).

[7] Navarra, G., Antoni, T., Apel, W., et al. 'KASCADE-Grande: a large acceptance, high-resolution cosmic-ray detector up to 10^{18} eV'. *Nuclear Instruments and Methods in Physics Research A* **518**, 207 (2004).

[8] Khristiansen, G. B., Formin, Y. A., Kalmykov, N. N., et al. 'The Primary Cosmic Ray Mass Composition Around the Knee of the Energy Spectrum'. *Nuclear Physics B (Proceedings Supplemental)* **39A**, 235 (1995).

[9] Horandel, J. R. 'On the Knee in the Energy Spectrum of Cosmic Rays'. *Astroparticle Physics* **19**(2), 193 (2003).

[10] Candia, J., Epele, L., and Roulet, E. 'Cosmic Ray photodisintegration and the knee of the spectrum'. *astro-ph* **0011010** (2000).

[11] Bird, D., Corbato, S. C., Dai, H. Y., et al. 'Evidence for Correlated Changes in the Spectrum and Composition of Cosmic Rays at Extremely High Energies'. *Physical Review Letters* **71**, 3401 (1993).

[12] Baltrusaitis, R., Cady, R., Cassiday, G., et al. 'The Utah Fly's Eye Detector'. *Nuclear Instruments and Methods in Physics Research A* **240**, 410 (1985).

[13] Abu-Zayyad, T., Al-Seady, M., Belov, K., et al. 'The prototype high-resolution Fly's Eye cosmic ray detector'. *Nuclear Instruments and Methods in Physics Research Section A* **450**(2-3), 253 (2000).

[14] Chiba, N., Hashimoto, K., Hayashida, N., et al. 'Akeno Giant Air Shower Array (AGASA) covering 100 km^2 area'. *Nuclear Instruments and Methods in Physics Research Section A* **311**, 338 (1992).

[15] The Pierre Auger Collaboration. 'Properties and Performance of the Prototype Instrument for the Pierre Auger Observatory'. *Nuclear Instruments and Methods in Physics Research A* **523**, 50 (2004).

[16] Artamonov, V., Afanasiev, B., Glushkov, A., et al. 'Present state and outlook of the Yakutsk EAS array'. *Bulletin of the Russian Academy of Sciences Physics* **58**(12), 2026 (1994).

[17] Bellido, J. A., Clay, R. W., Dawson, B. R., et al. 'Southern Hemisphere Observations of a 10^{18} eV Cosmic Ray Source Near the Direction of the Galactic Centre'. *Astroparticle Physics* **15**, 167 (2001).

[18] Tennent, R. 'The haverah park extensive air shower array'. *Proceedings of the Physical Society* **92**, 622 (1967).

[19] Bunner, A. N. *Cosmic Ray Detection by Atmospheric Fluorescence*. PhD thesis, Cornell University, (1967).

[20] Greisen, K. 'End to the Cosmic Ray Spectrum?'. *Physical Review Letters* **16**, 748 (1966).

[21] Zatsepin, G. T. and Kuz'min, V. A. 'Upper Limit of the Energy Spectrum of Cosmic Rays'. *Journal of Experimental and Theoretical Physics Letters* **4**, 78 (1966).

[22] Baltrusaitis, R., Cady, R., Cassiday, G., et al. 'Evidence for a High-Energy Cosmic Ray Spectrum Cutoff'. *Physical Review Letters* **54**(16), 1875 (1985).

[23] Abbasi, R. U., Abu-Zayyad, T., Amann, J. F., et al. 'Measurement of the flux of ultrahigh energy cosmic rays from monocular observations by the high resolution fly's eye experiment'. *Physical Review Letters* **92**, 151101 (2004).

[24] Abbasi, R. U., Abu-Zayyad, T., Amman, J. F., et al. 'Monocular measurement of the spectrum of UHE cosmic rays by the FADC detector of the HiRes experiment'. *Astroparticle Physics* **23**, 157 (2005).

[25] Takeda, M., Sakaki, N., Honda, K., et al. 'Energy determination in the Akeno Giant Air Shower Array experiment'. *Astroparticle Physics* **19**, 447 (2003).

[26] Connolly, B., BenZvi, S., Finley, C., et al. 'Comparison of the Ultra-High Energy Cosmic Ray Flux Observed by AGASA, HiRes and Auger'. *Physical Review D* **74**(4), 43001 (2006).

[27] Bird, D. 'Detection of a cosmic ray with measured energy well beyond the expected spectral cut off due to cosmic microwave radiation'. *Astrophysical Journal* **441**, 144 (1995).

[28] Hayashida, K., Honda, K., Honda, M., et al. 'Observation of a very energetic Cosmic Ray well beyond the predicted 2.7 K Cutoff in the primary energy spectrum'. *Physical Review Letters* **73**(26), 3491 (1994).

[29] Takeda, M., Hayashida, N., Honda, K., et al. 'Small-Scale Anisotropy of Cosmic Rays above 10^{19} eV Observed with the Akeno Giant Air Shower Array'. *Astrophysical Journal* **522**, 225 (1999).

[30] Hayashida, N., Nagano, M., Nishikawa, D., et al. 'The anisotropy of cosmic ray arrival directions around 10^{18} eV'. *Astroparticle Physics* **10**(4), 303 (1999).

[31] Abbasi, R. U., Abu-Zayyad, T., Amann, J. F., et al. 'Study of Small-Scale Anisotropy of UltraHigh-Energy Cosmic Rays Observed in Stereo by the High Resolution Fly's Eye Detector'. *Astrophysical Journal* **610**(2), L73 (2004).

[32] Letessier-Selvon, A. and the Pierre Auger Collaboration. 'Anisotropy Studies Around the Galactic Center at EeV Energies with Auger Data'. In *29th International Cosmic Ray Conference*, volume 7, 67 (Tata Institute of Fundamental Research, Pune, 2005).

[33] Abu-Zayyad, T., Belov, K., Bird, D. J., et al. 'Measurement of the Cosmic-Ray Energy Spectrum and Composition from 10^{17} to $10^{18.3}$ eV Using a Hybrid Technique'. *Astrophysical Journal* **557**, 686 (2001).

[34] Bhattacharjee, P. and Sigl, G. 'Origin and Propagation of Extremely High Energy Cosmic Rays'. *Physics Reports* **327**, 109 (2000).

[35] Dawson, B. R., Meyhandan, R., and Simpson, K. M. 'A comparison of cosmic ray composition measurements at the highest energies'. *Astroparticle Physics* **9**, 331 (1998).

[36] Hayashida, N., Honda, K., Honda, M., et al. 'Muons (¿or=1 GeV) in large extensive air showers of energies between $10^{16.5}$ eV and $10^{19.5}$ eV observed at Akeno'. *J. Phys. G, Nucl. Part. Phys. (UK)* **21**(8), 1101 (1995).

[37] Yoshida, S. and Dai, H. 'The extremely high energy cosmic rays'. *J. Phys. G, Nucl. Part. Phys. (UK)* **24**(5), 905–938 (1998).

[38] Protheroe, R. J. and Clay, R. W. 'Ultra High Energy Cosmic Rays'. *Publications of the Astronomical Society of Australia* **21**, 1 (2004).

[39] Fransson, C. and Bjornsson, C. I. 'Radio emission and particle acceleration in SN 1993J'. *Astrophysical Journal* **509**, 861 (1998).

[40] Hillas, A. M. 'Can diffusive shock acceleration in supernova remnants account for high-energy galactic cosmic rays?'. *Journal of Physics G: Nuclear Physics* **31**, R95 (2005).

[41] Rachen, J. P. and Biermann, P. L. 'Extragalactic ultra high energy cosmic rays; I. Contribution from hot spots in FR-II Radio Galaxies'. *Asronomy and Astrophysics* **272**, 161 (1993).

[42] Rossi, B. *Cosmic Rays*. McGraw-Hill, New York, (1964).

[43] Gaisser, T. K. and Hillas, A. M. 'Reliability of the method of constant intensity cuts for reconstructing the average development of vertical showers'. In *15th International Cosmic Ray Conference*, volume 8, 353 (, Plovdiv, Bulgaria, 1977).

[44] Nagano, M., Kobayakawa, K., Sakaki, N., et al. 'New measurement on photon yields from air and the application to the energy estimation of primary cosmic rays'. *Astroparticle Physics* **22**, 235 (2004).

[45] Jelley, J. *Cherenkov Radiation and its Applications*. Pergamon Press, 1 edition, (1958).

[46] Nerling, F., Engel, R., Guerard, C., et al. 'Analytical versus Monte Carlo Description of Cherenkov Contribution in Air Showers'. In *28th International Cosmic Ray Conference*, volume 2, 611 (Institute for Cosmic Ray Research, Tsukuba, 2003).

[47] Hillas, A. M. 'Angular and Energy Distributions of Charged Particles in Electron-photon cascades in air'. *Journal of Physics G: Nuclear Physics* **8**, 1461 (1982).

[48] Hillas, A. M. 'The Sensitivity of Cherenkov radiation pulses to the longitudinal development of cosmic-ray showers'. *Journal of Physics G: Nuclear Physics* **8**, 1475 (1982).

[49] McCartney, E. J. *Optics of the Atmosphere, Scattering by Molecules and Particles*. John Wiley and Sons, Inc., United States of America, (1976).

[50] Matthews, J., Wiencke, L., and Dawson, B. 'Proposed Atmospheric Monitoring for HiRes Experiment'. *www.physics.utah.edu/ sommers/hybrid/papers/index.html* (1998).

[51] Roberts, M. D. 'The role of atmospheric multiple scattering in the transmission of fluorescence light from extensive air showers'. *Journal of Physics G: Nuclear Physics* **31**(11), 1291 (2005).

[52] Simpson, K. M. *Studies of Cosmic Ray Compostion using a Hybrid Fluorescence Detector*. Doctor of philosophy, University of Adelaide, (2001).

[53] The Pierre Auger Collaboration. 'The Pierre Auger Project Collaboration Design Report'. Technical report, (1995).

[54] Matthiae, G. 'Optics and Mechanics of the Auger Fluorescence Detector'. *Internal GAP Note* **037** (2001).

[55] Palatka, M., Hrabovsky, M., Schovanek, P., et al. 'Bifocal Optical System of the Schmidt Camera. (Design of the Corrector Ring)'. *Internal GAP Note* **002** (2000).

[56] Gemmeke, H. 'The Auger Fluorescence Detector Electronics'. *Internal GAP Note* **030** (2001).

[57] Argiro, S., Barroso, S. L. C., Gonzalez, J., et al. 'The Offline software framework of the Pierre Auger Observatory'. *IEEE Nuclear Science Symposium Conference* , 1000 (2006).

[58] Keilhauer, B., Klages, H., and Risse, M. 'Results of the first balloon measurements above the Pampa Amarilla'. *Internal GAP Note* **009** (2003).

[59] Roberts, M. D. 'Atmospheric characterisation for the Auger fluorescence detector using vertical laser beams'. *Internal GAP Note* **056** (2001).

[60] Cester, R., Mostafa, M., and Mussa, R. 'LIDAR Telescopes for Atmosperic Monitoring'. *Internal GAP Note* **052** (2001).

[61] Klett, J. D. 'Stable analytical inversion solution for processing lidar returns'. *Applied Optics* **20**, 211 (1981).

[62] Klett, J. D. 'Lidar inversion with variable backscatter/extinction ratios'. *Applied Optics* **24**, 1638 (1985).

[63] Fernald, F. G. 'Analysis of atmospheric lidar observations: some coments'. *Applied Optics* **23**, 652 (1984).

[64] Biral, A., Medina Tanco, G. A., Reis, H. C., et al. 'Proposal of an Additional Atmospheric Monitoring System for the Auger Site'. *Internal GAP Note* **023** (2002).

[65] Stanev, T. *High Energy Cosmic Rays.* Praxis, Chichester, UK, (2004).

[66] Sommers, P. 'First Estimate of the Primary Cosmic Ray Energy Spectrum above 3 EeV from the Pierre Auger Observatory'. In *25th International Cosmic Ray Conference*, volume 7, 387 (Tata Institute of Fundamental Research, Pune, 2005).

[67] Brack, J., Meyhandan, R., and Hofman, G. 'Prototype Auger Absolute Calibration System: Fluorescence Detector Calibration at Los Leones'. *Internal GAP Note* **033** (2002).

[68] Roberts, M. D., Sommers, P., and Fick, B. 'Ultra Local Phase Function Measurements'. *Internal GAP Note* **059** (2000).

[69] Song, C., Cao, Z., Dawson, B., et al. 'Energy Estimation of UHE Cosmic Rays using the Atmospheric Fluorescence Technique'. *Astroparticle Physics* **14**, 7 (2000).

[70] Argiro, S. and Capoa, A. d. 'FlOReS; The Fluorescent Detector Offline Reconstruction System; Project Design Overview version 1.0'. (2001).

[71] Heck, D., Knapp, J., Capdevielle, J., et al. *CORSIKA: A Monte Carlo Code to Simulate Extensive Air Showers*. FORSCHUNGSZENTRUM KARLSRUHE Technikund Umwelt, (1998).

[72] Prado, J. L., Dawson, B., Petrera, S., et al. 'Simulation of the fluorescence detector of the Pierre Auger Observatory'. *Nuclear Instruments and Methods in Physics Research A* **545**, 632 (2005).

[73] Jelley, J. 'Cherenkov Radiation from Extensive Air Showers'. *Progression in Elementary Particle and Cosmic Ray Physics* **9**, 96 (1967).

[74] Dawson, B. and Sommers, P. 'The Hybrid Aperture and Precision of the Auger Observatory'. In *27th International Cosmic Ray Conference*, volume 2, 714 (German Physical Society, Hamburg, 2001).

[75] Baltrusaitis, R., Cassiday, G., Cooper, R., et al. 'Measurement of the Angular Distribution of Cherenkov Light in Ultra-High Energy Extensive Air Showers'. *Journal of Physics G: Nuclear Physics* **13**, 115 (1987).

[76] Nerling, F. 'Description of Cherenkov light production in Extensive Air Showers'. *Internal GAP Note* **063** (2005).

Appendix A

Tables of the output from the Flores version of AerosolMin

These Tables document all of the values of the VAOD that was found by the Flores version of AerosolMin when the 144 simulated events were reconstructed. For the lower energy events, the noise present in the Coihueco detector disrupts the ability of AerosolMin to accurately calculate the VAOD, especially when the aerosol concentration in the atmosphere is high (VAOD is low), see Chapter 5. All the values of the $VAOD$ and horizontal attenuation length are defined from the height of the detector.

Energy = 10^{19} eV

	Initial VAOD = 0.04					
Event No.	Number of Bins	χ^2	Normalised χ^2	$\Lambda_a(\lambda)$ (m)	h_a (m)	$VAOD$
1	118	100.32	0.85	40000	1200	0.030
2	111	111.24	1.00	40000	1200	0.030
3	104	127.16	1.22	19000	1200	0.063
4	93	100.69	1.08	13000	1200	0.092
5	101	169.28	1.68	12000	1200	0.100
6	75	129.16	1.72	11000	1200	0.109
7	49	78.97	1.61	7000	1200	0.171
8	89	103.10	1.16	6000	1200	0.200
9	17	16.34	0.96	21000	1200	0.057
10	60	59.57	0.99	19000	1200	0.063
11	0	0.00	∞	5000	1200	0.240
12	0	0.00	∞	5000	1200	0.240
13	0	0.00	∞	5000	1200	0.240
14	0	0.00	∞	5000	1200	0.240
15	0	0.00	∞	5000	1200	0.240
16	0	0.00	∞	5000	1200	0.240
	Initial VAOD = 0.07					
Event No.	Number of Bins	χ^2	Normalised χ^2	$\Lambda_a(\lambda)$ (m)	h_a (m)	$VAOD$
1	131	140.73	1.07	5000	1200	0.240
2	128	117.17	0.92	40000	1200	0.030
3	100	90.83	0.91	11000	1200	0.109
4	93	109.89	1.18	5000	1200	0.240
5	71	56.85	0.80	11000	1200	0.109
6	56	71.27	1.27	17000	1200	0.071
7	0	0.00	∞	5000	1200	0.240
8	0	0.00	∞	5000	1200	0.240
9	0	0.00	∞	5000	1200	0.240
10	0	0.00	∞	5000	1200	0.240
11	0	0.00	∞	5000	1200	0.240
12	0	0.00	∞	5000	1200	0.240
13	0	0.00	∞	5000	1200	0.240
14	0	0.00	∞	5000	1200	0.240
15	0	0.00	∞	5000	1200	0.240
16	0	0.00	∞	5000	1200	0.240
	Initial VAOD = 0.10					
Event No.	Number of Bins	χ^2	Normalised χ^2	$\Lambda_a(\lambda)$ (m)	h_a (m)	$VAOD$
1	120	148.50	1.24	5000	1200	0.240
2	95	162.98	1.72	5000	1200	0.240
3	91	80.78	0.89	40000	1200	0.030
4	59	62.55	1.06	24000	1200	0.050
5	101	101.20	1.00	15000	1200	0.080
6	0	0.00	∞	5000	1200	0.240
7	0	0.00	∞	5000	1200	0.240
8	0	0.00	∞	5000	1200	0.240
9	0	0.00	∞	5000	1200	0.240
10	0	0.00	∞	5000	1200	0.240
11	0	0.00	∞	5000	1200	0.240
12	0	0.00	∞	5000	1200	0.240
13	0	0.00	∞	5000	1200	0.240
14	0	0.00	∞	5000	1200	0.240
15	0	0.00	∞	5000	1200	0.240
16	0	0.00	∞	5000	1200	0.240

Table A.1:

Energy = $10^{19.5}$ eV

	Initial VAOD = 0.04					
Event No.	Number of Bins	χ^2	Normalised χ^2	$\Lambda_a(\lambda)$ (m)	h_a (m)	$VAOD$
1	141	116.07	0.82	5000	1200	0.240
2	130	155.45	1.20	40000	1200	0.030
3	155	174.74	1.13	18000	1200	0.067
4	134	132.24	0.99	15000	1200	0.080
5	100	111.61	1.12	28000	1200	0.043
6	145	231.95	1.60	18000	1200	0.067
7	126	192.27	1.53	17000	1200	0.071
8	119	159.33	1.34	25000	1200	0.048
9	105	122.09	1.16	17000	1200	0.071
10	106	138.97	1.31	18000	1200	0.067
11	97	109.68	1.13	19000	1200	0.063
12	91	93.49	1.03	19000	1200	0.063
13	80	154.10	1.93	5000	1200	0.240
14	0	0.00	∞	5000	1200	0.240
15	0	0.00	∞	5000	1200	0.240
16	0	0.00	∞	5000	1200	0.240
	Initial VAOD = 0.07					
Event No.	Number of Bins	χ^2	Normalised χ^2	$\Lambda_a(\lambda)$ (m)	h_a (m)	$VAOD$
1	167	117.01	0.70	40000	1200	0.030
2	157	181.31	1.15	11000	1200	0.109
3	146	132.10	0.90	12000	1200	0.100
4	109	105.11	0.96	15000	1200	0.080
5	123	167.85	1.36	14000	1200	0.086
6	126	147.46	1.17	12000	1200	0.100
7	88	114.34	1.30	8000	1200	0.150
8	111	113.38	1.02	12000	1200	0.100
9	100	117.44	1.17	13000	1200	0.092
10	125	162.59	1.30	8000	1200	0.150
11	93	156.17	1.68	8000	1200	0.150
12	111	104.04	0.94	12000	1200	0.100
13	0	0.00	∞	5000	1200	0.240
14	0	0.00	∞	5000	1200	0.240
15	0	0.00	∞	5000	1200	0.240
16	0	0.00	∞	5000	1200	0.240
	Initial VAOD = 0.10					
Event No.	Number of Bins	χ^2	Normalised χ^2	$\Lambda_a(\lambda)$ (m)	h_a (m)	$VAOD$
1	141	108.91	0.77	10000	1200	0.120
2	113	125.56	1.11	5000	1200	0.240
3	138	160.42	1.16	8000	1200	0.150
4	120	131.71	1.10	6000	1200	0.200
5	129	194.80	1.51	9000	1200	0.133
6	114	130.34	1.14	6000	1200	0.200
7	103	142.94	1.39	6000	1200	0.200
8	112	199.78	1.78	7000	1200	0.171
9	85	167.15	1.97	5000	1200	0.240
10	89	96.22	1.08	9000	1200	0.133
11	82	83.62	1.02	6000	1200	0.200
12	46	66.75	1.45	6000	1200	0.200
13	0	0.00	∞	5000	1200	0.240
14	0	0.00	∞	5000	1200	0.240
15	0	0.00	∞	5000	1200	0.240
16	0	0.00	∞	5000	1200	0.240

Table A.2:

Energy = 10^{20} eV

	Initial VAOD = 0.04					
Event No.	Number of Bins	χ^2	Normalised χ^2	$\Lambda_a(\lambda)$ (m)	h_a (m)	$VAOD$
1	157	156.55	1.00	40000	1200	0.030
2	176	221.45	1.26	40000	1200	0.030
3	172	224.63	1.31	40000	1200	0.030
4	153	227.42	1.49	40000	1200	0.030
5	158	189.27	1.20	40000	1200	0.030
6	146	197.42	1.35	40000	1200	0.030
7	145	166.19	1.15	28000	1200	0.043
8	142	166.09	1.17	27000	1200	0.044
9	139	184.36	1.33	29000	1200	0.041
10	138	158.71	1.15	31000	1200	0.039
11	123	106.34	0.86	34000	1200	0.035
12	111	150.76	1.36	27000	1200	0.044
13	97	487.90	5.03	26000	1200	0.046
14	80	509.42	6.37	40000	1200	0.030
15	69	389.14	5.64	40000	1200	0.030
16	53	346.15	6.53	40000	1200	0.030
	Initial VAOD = 0.07					
Event No.	Number of Bins	χ^2	Normalised χ^2	$\Lambda_a(\lambda)$ (m)	h_a (m)	$VAOD$
1	184	187.92	1.02	40000	1200	0.030
2	164	170.05	1.04	17000	1200	0.071
3	169	216.80	1.28	15000	1200	0.080
4	130	169.78	1.31	16000	1200	0.075
5	171	228.13	1.33	17000	1200	0.071
6	154	190.75	1.24	18000	1200	0.067
7	145	195.13	1.35	18000	1200	0.067
8	150	215.99	1.44	14000	1200	0.086
9	119	132.09	1.11	14000	1200	0.086
10	122	98.38	0.81	15000	1200	0.080
11	125	128.23	1.03	16000	1200	0.075
12	108	106.68	0.99	16000	1200	0.075
13	92	141.95	1.54	14000	1200	0.086
14	82	320.55	3.91	15000	1200	0.080
15	66	231.50	3.51	32000	1200	0.038
16	54	199.37	3.69	40000	1200	0.030
	Initial VAOD = 0.10					
Event No.	Number of Bins	χ^2	Normalised χ^2	$\Lambda_a(\lambda)$ (m)	h_a (m)	$VAOD$
1	164	146.48	0.89	40000	1200	0.030
2	154	217.19	1.41	13000	1200	0.092
3	172	234.05	1.36	13000	1200	0.092
4	136	156.17	1.15	9000	1200	0.133
5	151	202.74	1.34	10000	1200	0.120
6	152	188.56	1.24	11000	1200	0.109
7	98	122.27	1.25	10000	1200	0.120
8	140	165.27	1.18	10000	1200	0.120
9	151	163.47	1.08	10000	1200	0.120
10	129	191.27	1.48	10000	1200	0.120
11	122	435.29	3.57	10000	1200	0.120
12	97	110.59	1.14	11000	1200	0.109
13	95	212.43	2.24	11000	1200	0.109
14	83	211.94	2.55	12000	1200	0.100
15	65	159.90	2.46	22000	1200	0.055
16	53	117.32	2.21	12000	1200	0.100

Table A.3:

Appendix B

Conversion from $\Lambda_a(\lambda)$ to $VAOD$

Since the natural parameter used by the Offline program is $\Lambda_a(\lambda)$ at sea level and the values of the aerosol concentration recorded for the detector are in $VAOD$ from the height of the detector a conversion between the two is provided here.

First the $\Lambda_a(\lambda)_{sea\ level}$ at sea level must be converted to $\Lambda_a(\lambda)_{detector}$ from the height of the detector. This can be done by rearranging Equation 5.7,

$$\Lambda_a(\lambda)_{detector} = \Lambda_a(\lambda)_{sea\ level} \exp \frac{h}{h_a} \tag{B.1}$$

where h is the height of the detector and can be approximated to be 1.4 km.

Then the value of the $VAOD$ can be found by using Equation 5.3,

$$VAOD = \frac{h_a}{\Lambda_a(\lambda)} \tag{B.2}$$

Since this conversion is most relevant to the values of aerosol attenuation length quoted in Chapter 7, a table of the explicit relationship between the $\Lambda_a(\lambda)$ at sea level to the $VAOD$ from the height of the detector is given below.

$\Lambda_a(\lambda)$	$VAOD$
49	0.005
25	0.01
12	0.02
8	0.03
6	0.04
5	0.05
4	0.06
3	0.08
2.5	0.10
1.5	0.15

Table B.1: Conversion from $\Lambda_a(\lambda)$ at sea level, in meters to the dimensionless $VAOD$ from the height of the detector.

Appendix C

Parameters from the Coihueco Data Chain

The values of X_{max}, N_{max} and inital cosmic ray energy as reconstructed from the data collected by the Coihueco fluorescence detector are shown in this Appendix. These values correspond to the surface plots seen in Chapter 7, through Table 7.1 and the Equations 7.11 and 7.12. The difference between the values reconstructed by the two data chains, as plotted in Chapter 7, are always taken to be positive. The aerosol attenuation lengths quoted in this Appendix are all defined from sea level and the conversion to the $VAOD$ at the height of the detector can be found in Appendix B.

$\Delta\chi_0(^\circ)$	Aerosol Attenuation Length (km)									
	49	25	12	8	6	5	4	3	2.5	1.5
-1.0	701	701	701	701	701	0	0	0	0	0
-0.9	701	701	701	1027	1024	1024	1023	1024	1025	1030
-0.8	701	701	998	997	997	997	997	998	0	0
-0.7	701	988	986	984	984	983	984	985	986	991
-0.6	701	957	955	954	954	954	955	957	959	965
-0.5	701	944	941	940	940	941	941	943	946	952
-0.4	926	920	918	918	918	918	919	922	924	931
-0.3	905	899	898	898	899	901	902	905	909	918
-0.2	885	879	878	0	880	881	883	887	890	899
-0.1	863	858	857	858	860	861	863	867	871	881
0.0	843	838	838	839	841	843	845	850	854	865
0.1	820	815	815	817	819	822	824	829	834	845
0.2	799	794	796	798	800	803	806	811	816	828
0.3	775	771	773	775	778	781	784	790	796	809
0.4	755	753	756	760	763	767	770	776	782	795
0.5	736	733	736	740	743	747	750	757	763	776
0.6	718	715	719	723	726	730	734	741	747	761
0.7	703	703	707	711	715	719	723	730	736	750
0.8	678	678	682	686	690	695	698	706	712	727
0.9	667	668	673	678	682	686	690	698	704	719
1.0	645	645	650	654	659	663	667	675	682	698

Table C.1: Calculation of X_{max} in (g/cm^2) by the Coihueco reconstruction chain when the Hillas parameterisation of Cherenkov light production in an EAS is used.

$\Delta\chi_0(^\circ)$	Aerosol Attenuation Length (km)									
	49	25	12	8	6	5	4	3	2.5	1.5
-1.0	701	701	701	0	1023	1024	1022	1024	1026	1032
-0.9	701	701	1011	1010	1010	1010	1011	1012	1014	1020
-0.8	701	985	983	983	983	983	984	986	989	996
-0.7	701	971	969	969	969	969	970	972	975	981
-0.6	701	940	939	939	940	941	942	945	948	956
-0.5	932	926	925	925	925	926	928	931	934	942
-0.4	908	902	902	902	903	904	906	909	913	921
-0.3	888	882	882	883	885	887	889	893	898	908
-0.2	867	862	862	863	865	867	870	874	879	890
-0.1	846	841	842	844	846	849	851	856	861	872
0.0	827	822	823	826	828	831	834	839	844	857
0.1	804	800	802	804	807	810	813	819	824	837
0.2	785	781	783	786	789	792	795	801	807	821
0.3	762	758	761	764	768	771	775	781	788	801
0.4	743	743	746	750	754	758	761	768	774	789
0.5	726	724	728	731	735	739	743	749	756	770
0.6	709	708	712	716	720	723	727	734	741	756
0.7	695	696	701	705	709	713	717	724	731	746
0.8	673	673	678	682	686	690	694	702	708	724
0.9	663	665	670	674	679	683	687	694	701	716
1.0	643	643	648	653	657	661	665	673	680	696

Table C.2: Calculation of X_{max} in (g/cm^2) by the Coihueco reconstruction chain when the Nerling parameterisation of Cherenkov light production in an EAS is used.

$\Delta\chi_0(^\circ)$	Aerosol Attenuation Length (km)									
	49	25	12	8	6	5	4	3	2.5	1.5
-1.0	4.65	4.27	4.54	4.93	5.37	0.00	0.00	0.00	0.00	0.00
-0.9	4.77	4.48	4.78	7.88	9.51	10.47	11.52	13.88	16.65	25.92
-0.8	4.85	4.68	7.56	8.35	9.22	10.16	11.17	13.44	0.00	0.00
-0.7	5.03	6.78	7.51	8.29	9.14	10.06	11.06	13.28	15.90	24.57
-0.6	5.22	6.56	7.27	8.03	8.85	9.74	10.70	12.84	15.35	23.65
-0.5	5.41	6.53	7.23	7.98	8.79	9.67	10.61	12.71	15.17	23.30
-0.4	6.23	6.59	7.29	8.04	8.84	9.71	10.64	12.72	15.15	23.14
-0.3	6.00	6.35	7.02	7.74	8.52	9.36	10.26	12.26	14.60	22.29
-0.2	5.96	6.31	6.97	0.00	8.45	9.26	10.14	12.10	14.38	21.85
-0.1	5.99	6.34	7.00	7.70	8.45	9.26	10.13	12.06	14.31	21.65
0.0	5.93	6.27	6.91	7.60	8.34	9.13	9.97	11.85	14.04	21.16
0.1	5.83	6.16	6.78	7.45	8.16	8.92	9.74	11.56	13.66	20.51
0.2	5.81	6.14	6.75	7.40	8.10	8.85	9.65	11.43	13.48	20.16
0.3	5.62	5.94	6.52	7.15	7.82	8.53	9.30	10.99	12.96	19.31
0.4	5.63	5.92	6.48	7.09	7.74	8.44	9.19	10.85	12.77	18.97
0.5	5.63	5.93	6.49	7.09	7.73	8.41	9.14	10.76	12.63	18.65
0.6	5.66	5.95	6.50	7.09	7.71	8.39	9.11	10.70	12.53	18.42
0.7	5.56	5.83	6.35	6.92	7.53	8.18	8.87	10.41	12.18	17.88
0.8	5.66	5.93	6.45	7.00	7.60	8.24	8.92	10.43	12.16	17.71
0.9	5.53	5.77	6.27	6.80	7.38	7.99	8.65	10.10	11.78	17.12
1.0	5.63	5.87	6.36	6.89	7.45	8.05	8.70	10.12	11.76	16.97

Table C.3: Calculation of N_{max} in ($\times 10^{10}$ particles) by the Coihueco reconstruction chain when the Hillas parameterisation of Cherenkov light production in an EAS is used.

$\Delta\chi_0(^\circ)$	Aerosol Attenuation Length (km)									
	49	25	12	8	6	5	4	3	2.5	1.5
-1.0	5.08	4.71	5.00	0.00	8.95	9.85	11.85	14.26	17.10	26.59
-0.9	5.20	4.91	7.99	8.82	9.72	10.69	11.74	14.11	16.89	26.19
-0.8	5.27	7.04	7.78	8.58	9.45	10.39	11.41	13.70	16.38	25.30
-0.7	5.45	7.00	7.74	8.53	9.38	10.31	11.31	13.54	16.17	24.87
-0.6	5.63	6.81	7.53	8.30	9.12	10.02	10.98	13.14	15.67	24.01
-0.5	6.43	6.79	7.50	8.26	9.07	9.95	10.90	13.02	15.50	23.66
-0.4	6.51	6.87	7.57	8.33	9.14	10.01	10.95	13.05	15.49	23.52
-0.3	6.29	6.65	7.32	8.05	8.84	9.68	10.59	12.61	14.97	22.70
-0.2	6.27	6.62	7.29	8.00	8.77	9.60	10.48	12.46	14.76	22.28
-0.1	6.31	6.66	7.32	8.03	8.79	9.60	10.48	12.43	14.69	22.08
0.0	6.26	6.60	7.25	7.94	8.68	9.47	10.33	12.23	14.43	21.61
0.1	6.17	6.50	7.12	7.79	8.51	9.28	10.10	11.94	14.06	20.97
0.2	6.15	6.48	7.09	7.75	8.45	9.21	10.02	11.81	13.89	20.62
0.3	5.97	6.28	6.87	7.50	8.17	8.89	9.67	11.39	13.37	19.78
0.4	5.98	6.26	6.83	7.44	8.10	8.80	9.56	11.24	13.18	19.44
0.5	5.99	6.28	6.84	7.44	8.09	8.78	9.52	11.16	13.05	19.14
0.6	6.02	6.30	6.85	7.44	8.07	8.75	9.48	11.09	12.95	18.91
0.7	5.92	6.17	6.70	7.27	7.88	8.54	9.24	10.80	12.60	18.36
0.8	6.02	6.28	6.80	7.36	7.96	8.61	9.30	10.83	12.59	18.21
0.9	5.89	6.12	6.61	7.15	7.73	8.36	9.03	10.50	12.20	17.61
1.0	5.98	6.22	6.71	7.24	7.81	8.42	9.08	10.53	12.19	17.47

Table C.4: Calculation of N_{max} in ($\times 10^{10}$ particles) by the Coihueco reconstruction chain when the Nerling parameterisation of Cherenkov light production in an EAS is used.

$\Delta\chi_0(^\circ)$	Aerosol Attenuation Length (km)									
	49	25	12	8	6	5	4	3	2.5	1.5
-1.0	7.20	6.60	7.03	7.62	8.30	0.00	0.00	0.00	0.00	0.00
-0.9	7.38	6.92	7.40	14.65	17.65	19.43	21.37	25.73	30.88	48.09
-0.8	7.50	7.23	13.87	15.32	16.89	18.60	20.45	24.61	0.00	0.00
-0.7	7.78	12.38	13.69	15.11	16.65	18.31	20.11	24.16	28.92	44.74
-0.6	8.07	11.80	13.06	14.41	15.88	17.47	19.19	23.03	27.55	42.53
-0.5	8.36	11.66	12.89	14.22	15.66	17.22	18.89	22.65	27.05	41.60
-0.4	11.03	11.63	12.84	14.15	15.56	17.09	18.73	22.40	26.70	40.87
-0.3	10.50	11.07	12.24	13.50	14.85	16.32	17.89	21.42	25.53	39.10
-0.2	10.32	10.89	12.02	0.00	14.56	15.98	17.51	20.92	24.90	37.97
-0.1	10.24	10.80	11.92	13.12	14.41	15.80	17.30	20.63	24.51	37.23
0.0	10.03	10.57	11.65	12.81	14.06	15.41	16.85	20.07	23.82	36.08
0.1	9.72	10.24	11.28	12.40	13.59	14.88	16.26	19.34	22.91	34.56
0.2	9.57	10.08	11.09	12.17	13.34	14.59	15.93	18.91	22.38	33.65
0.3	9.13	9.61	10.57	11.60	12.70	13.88	15.15	17.97	21.24	31.85
0.4	9.02	9.47	10.39	11.39	12.46	13.61	14.84	17.58	20.75	31.04
0.5	8.91	9.37	10.27	11.24	12.27	13.39	14.58	17.22	20.28	30.17
0.6	8.85	9.29	10.16	11.11	12.12	13.20	14.37	16.94	19.92	29.51
0.7	8.61	9.01	9.85	10.76	11.73	12.77	13.89	16.37	19.23	28.44
0.8	8.61	9.01	9.82	10.70	11.65	12.66	13.74	16.13	18.89	27.76
0.9	8.35	8.71	9.49	10.33	11.24	12.21	13.25	15.55	18.19	26.69
1.0	8.35	8.71	9.47	10.28	11.16	12.10	13.11	15.33	17.89	26.07

Table C.5: Calculation of the initial cosmic ray energy in ($\times 10^{19}$ eV) by the Coihueco reconstruction chain when the Hillas parameterisation of Cherenkov light production in an EAS is used.

$\Delta\chi_0(^\circ)$	Aerosol Attenuation Length (km)									
	49	25	12	8	6	5	4	3	2.5	1.5
-1.0	7.85	7.28	7.72	0.00	16.62	18.29	21.96	26.43	31.70	49.38
-0.9	8.03	7.59	14.76	16.27	17.92	19.70	21.64	26.01	31.16	48.36
-0.8	8.15	12.83	14.17	15.62	17.20	18.91	20.77	24.93	29.84	46.18
-0.7	8.42	12.68	13.99	15.41	16.96	18.62	20.43	24.48	29.25	45.07
-0.6	8.70	12.15	13.41	14.77	16.24	17.84	19.56	23.42	27.95	42.96
-0.5	11.41	12.02	13.25	14.59	16.03	17.59	19.28	23.04	27.46	42.04
-0.4	11.41	12.01	13.22	14.54	15.96	17.48	19.13	22.82	27.13	41.34
-0.3	10.91	11.49	12.65	13.92	15.28	16.75	18.33	21.87	26.01	39.63
-0.2	10.75	11.31	12.45	13.68	15.00	16.42	17.96	21.38	25.38	38.50
-0.1	10.69	11.24	12.36	13.57	14.86	16.26	17.76	21.11	25.02	37.79
0.0	10.48	11.02	12.10	13.27	14.52	15.88	17.33	20.57	24.34	36.66
0.1	10.19	10.71	11.74	12.86	14.06	15.36	16.75	19.85	23.44	35.16
0.2	10.04	10.55	11.55	12.64	13.81	15.07	16.43	19.43	22.92	34.26
0.3	9.62	10.09	11.05	12.08	13.19	14.38	15.66	18.50	21.80	32.49
0.4	9.51	9.95	10.87	11.87	12.95	14.11	15.36	18.12	21.32	31.68
0.5	9.41	9.85	10.76	11.73	12.77	13.90	15.10	17.77	20.86	30.83
0.6	9.36	9.78	10.66	11.60	12.62	13.72	14.89	17.49	20.50	30.18
0.7	9.11	9.50	10.34	11.25	12.24	13.29	14.42	16.92	19.81	29.12
0.8	9.12	9.51	10.32	11.21	12.16	13.18	14.28	16.70	19.50	28.46
0.9	8.86	9.21	9.99	10.84	11.75	12.73	13.79	16.12	18.80	27.39
1.0	8.86	9.21	9.97	10.80	11.68	12.63	13.65	15.91	18.50	26.78

Table C.6: Calculation of the initial cosmic ray energy in ($\times 10^{19}$ eV) by the Coihueco reconstruction chain when the Nerling parameterisation of Cherenkov light production in an EAS is used.

Appendix D

Difference in the Reconstruction chains of two Detectors

The light profiles and difference in the reconstution of the Gaisser Hillas parameters and initial cosmic ray energy for the events at the GPS seconds of 799040826 and 770961669. The light profiles recorded the light collected by a detector, separated into the different components of light the Offline reconstuction software has calculated against an arbitrary time scale. The difference in the reconstruction of the Gaisser Hillas parameters and the initial cosmic ray energy were calculated for the various adjustments of the air shower geometry in the Coihueco detector around χ_0 by $\Delta\chi_0$ for the two events (see Chapter 7).

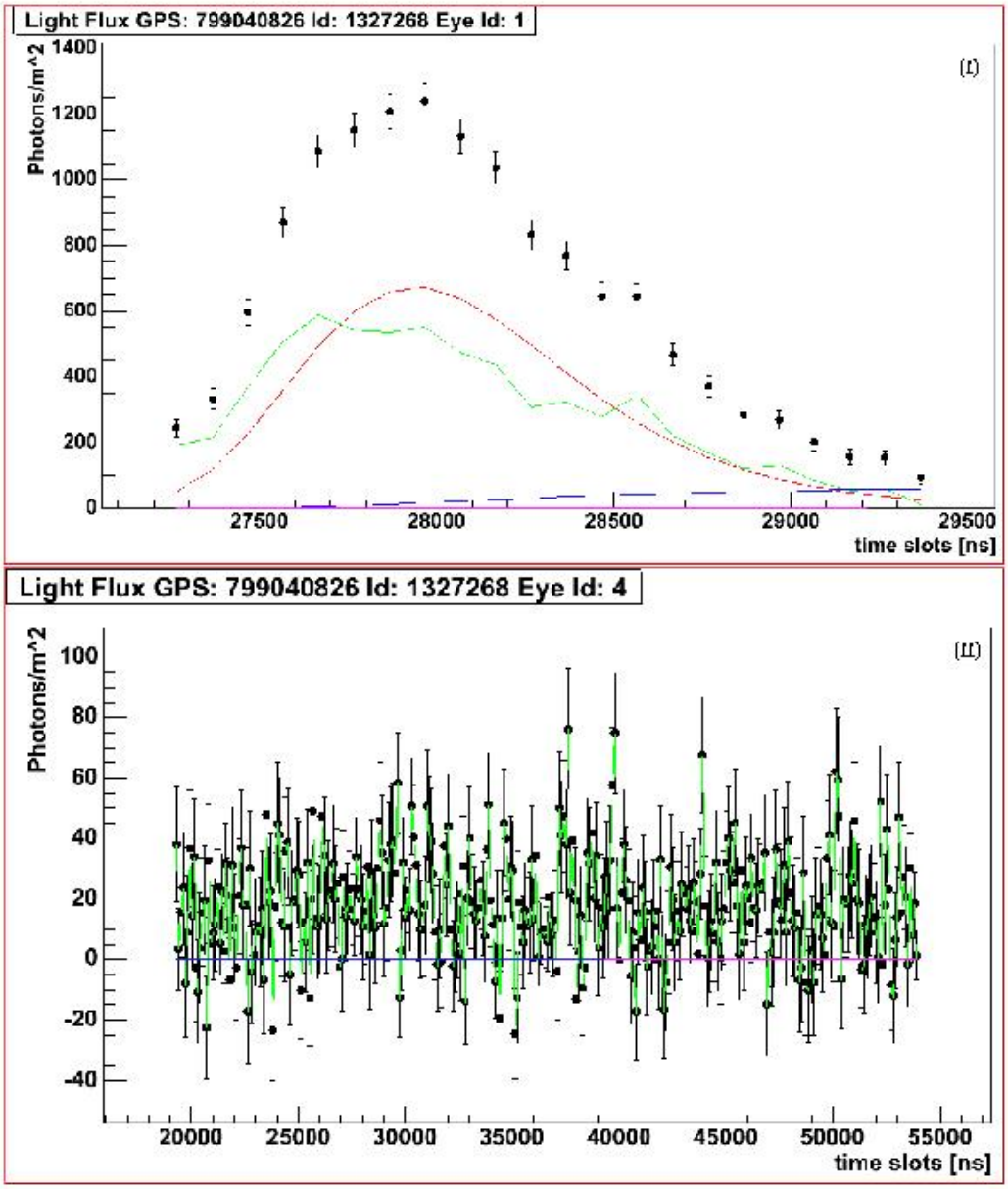

Figure D.1: The profiles of the light recorded by the detectors. Red-direct Cherenkov, blue-rayleigh scattered Cherenkov, pink-Mie scattered Cherenkov, green-fluorescence and black points are total light recorded. (i) is the Los Leones profile, (ii) is the Coihueco profile for event 799040826.

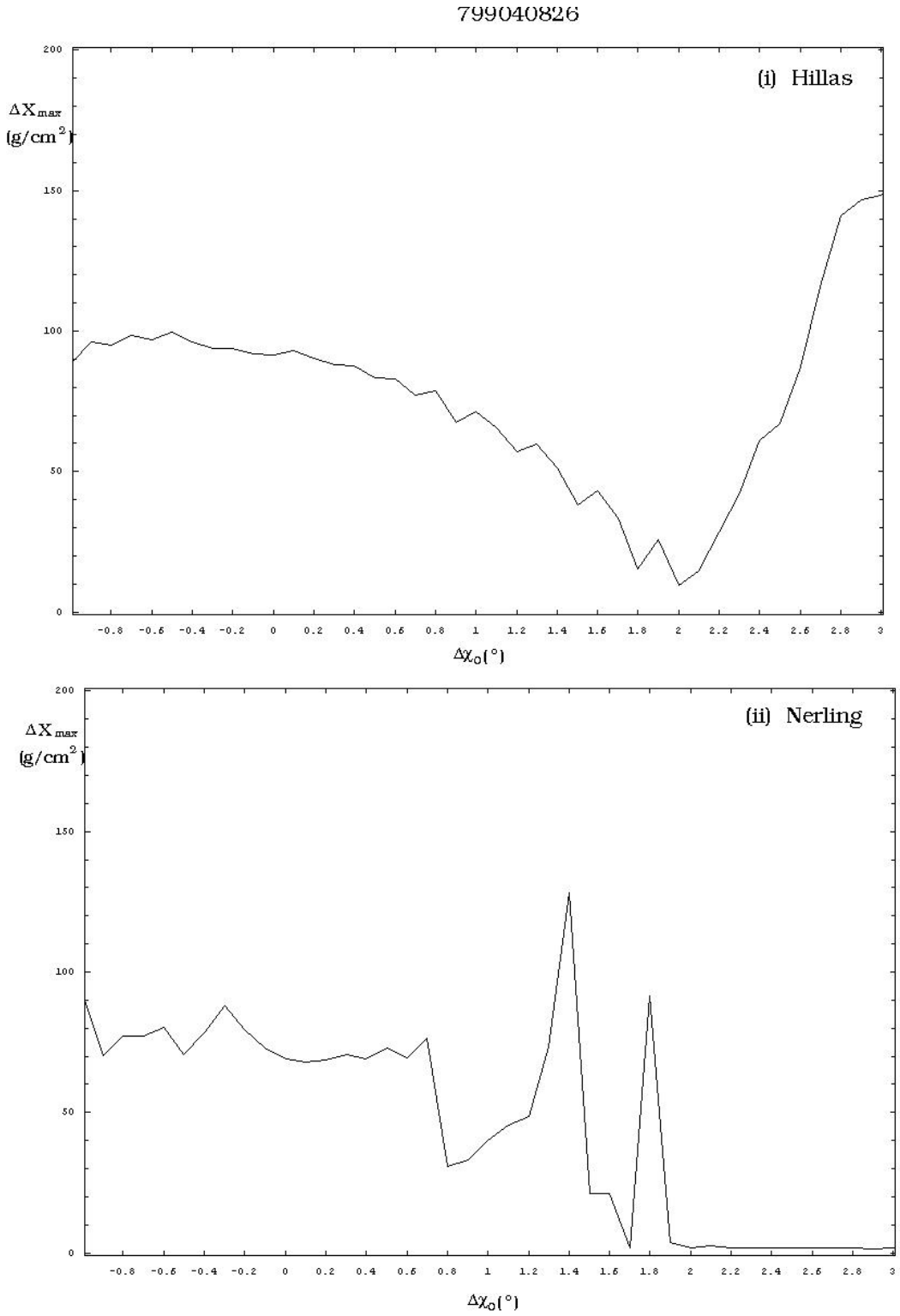

Figure D.2: Difference in the calculation of X_{max} between the two reconstruction chains that recorded the event (i) Hillas, (ii) Nerling

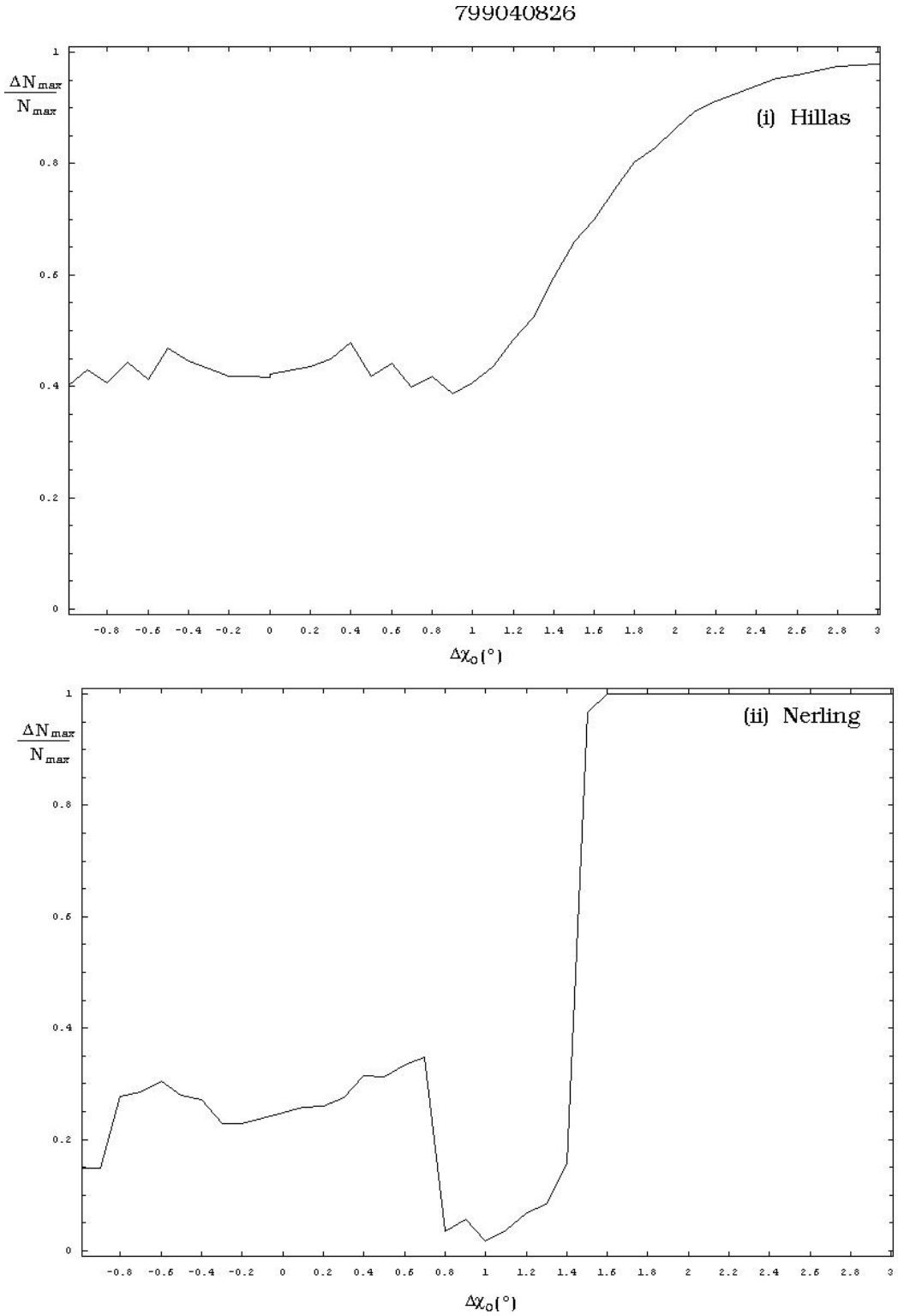

Figure D.3: Relative difference in the calculation of N_{max} between the two reconstruction chains that recorded the event (i) Hillas, (ii) Nerling

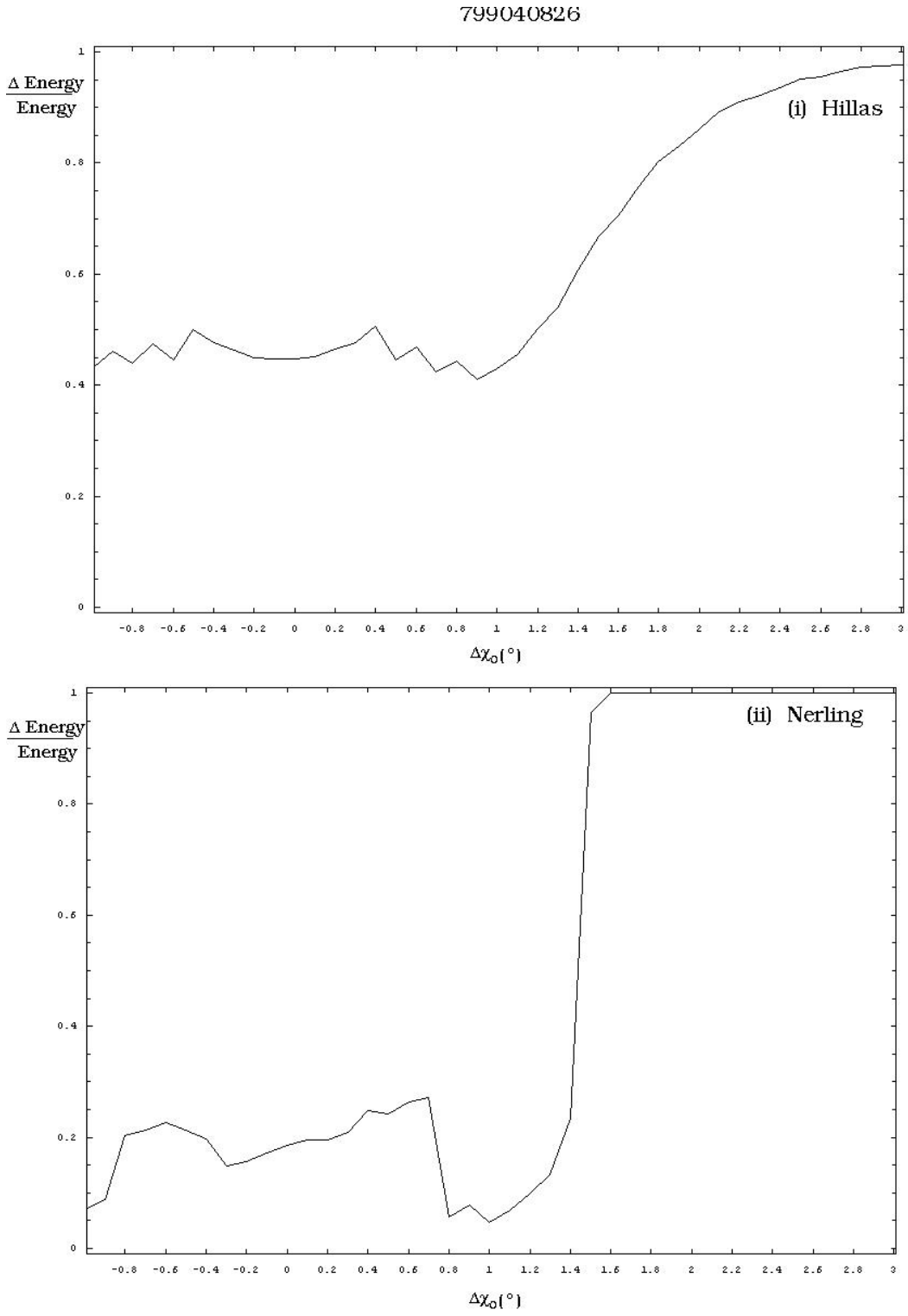

Figure D.4: Relative difference in the calculation of the initial energy between the two reconstruction chains that recorded the event (i) Hillas, (ii) Nerling

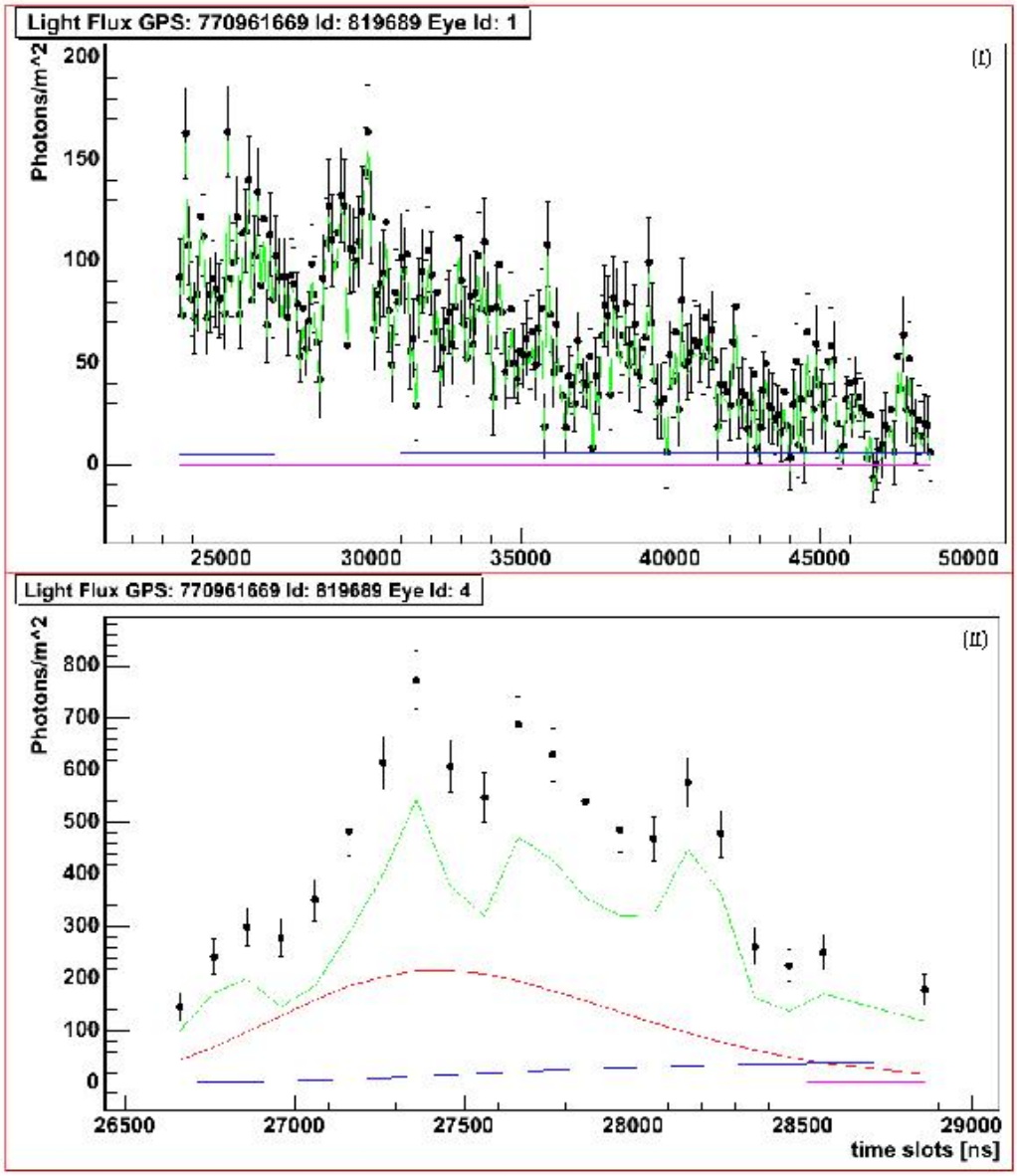

Figure D.5: The profiles of the light recorded by the detectors. Red-direct Cherenkov, blue-rayleigh scattered Cherenkov, pink-Mie scattered Cherenkov, green-fluorescence and black points are total light recorded. (i) is the Los Leones profile, (ii) is the Coihueco profile for event 770961669.

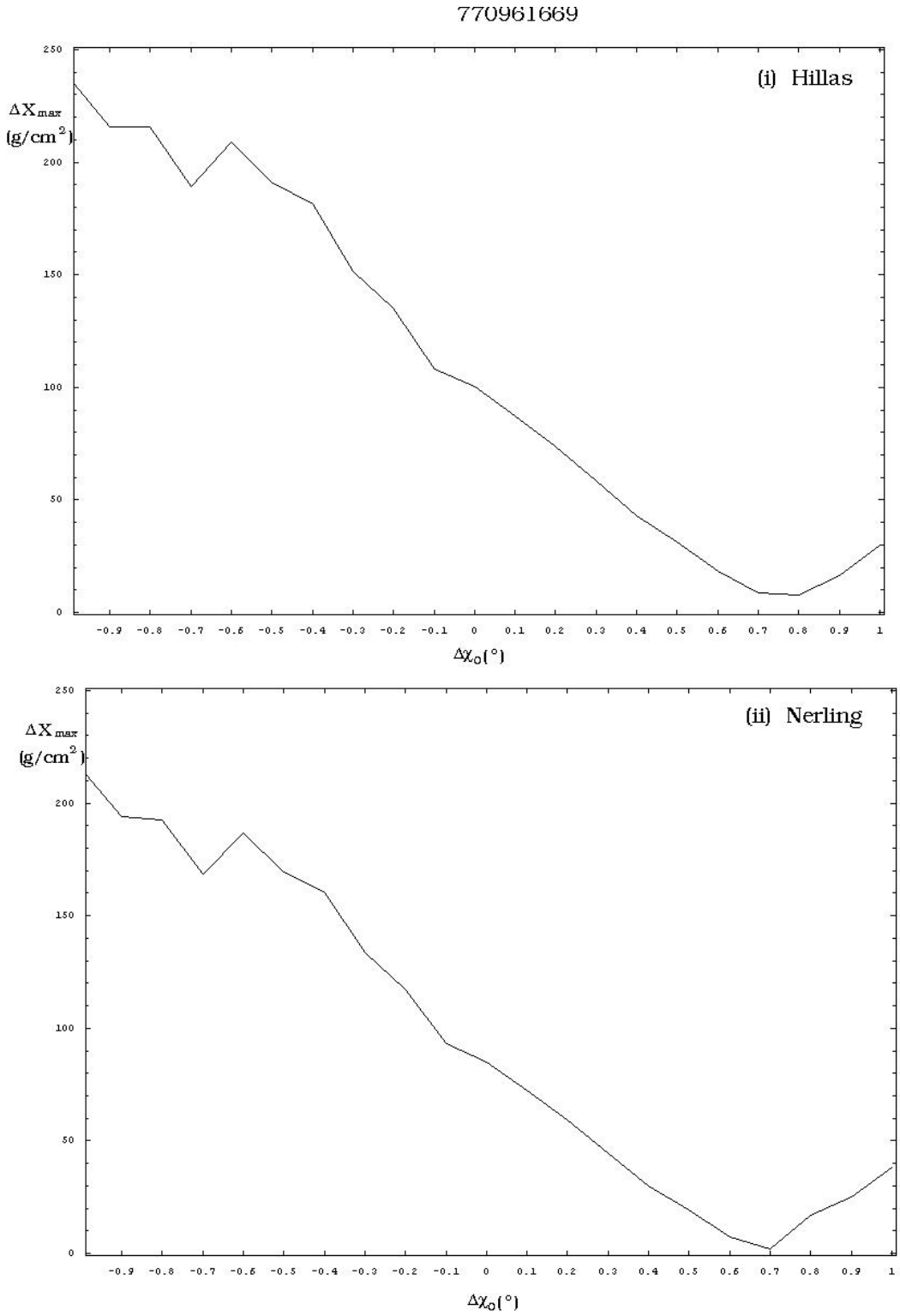

Figure D.6: Difference in the calculation of X_{max} between the two reconstruction chains that recorded the event (i) Hillas, (ii) Nerling

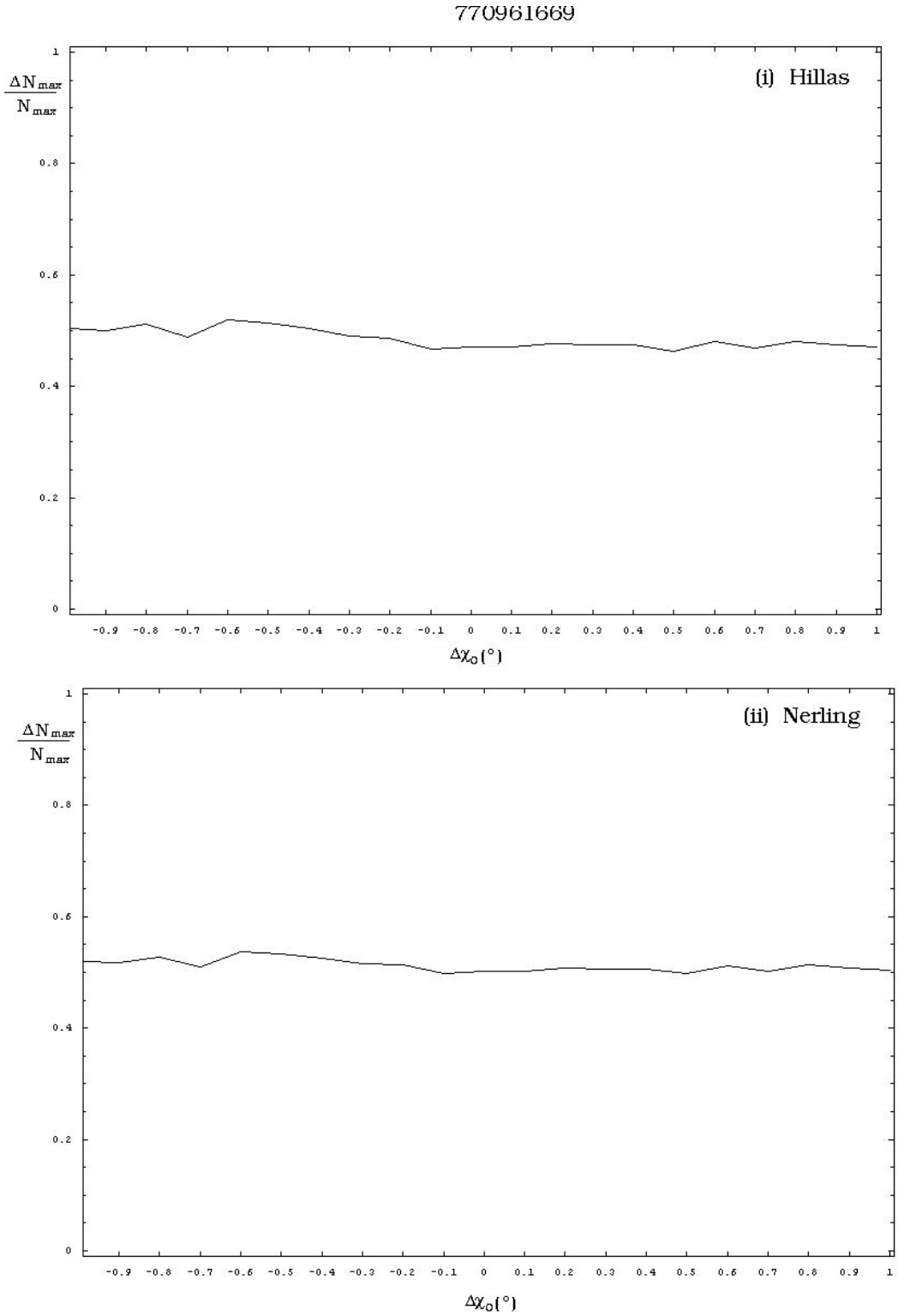

Figure D.7: Relative difference in the calculation of N_{max} between the two reconstruction chains that recorded the event (i) Hillas, (ii) Nerling

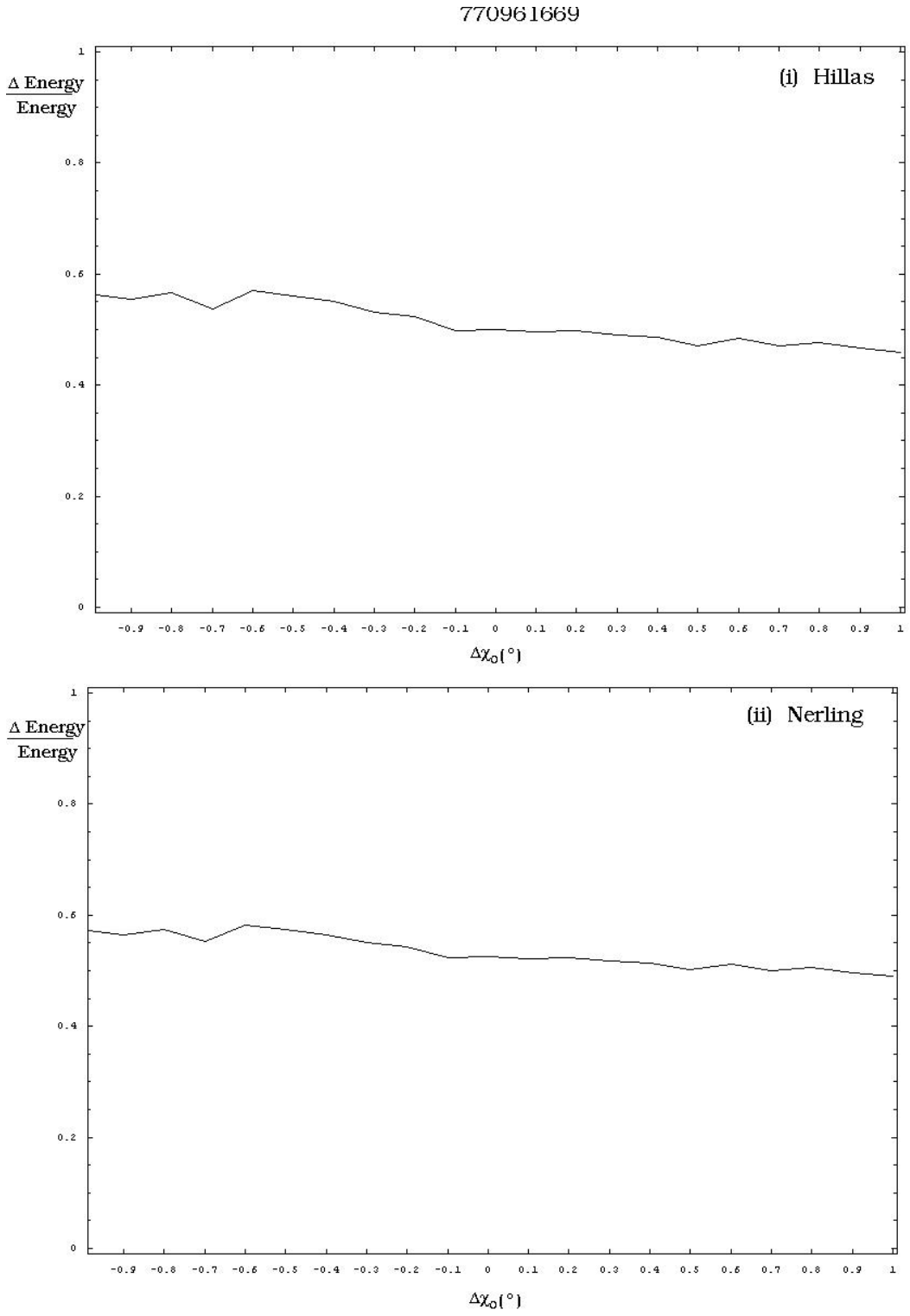

Figure D.8: Relative difference in the calculation of the initial energy between the two reconstruction chains that recorded the event (i) Hillas, (ii) Nerling